Supplementary Figures

A refined characterization of large-scale genomic differences in the first complete human genome

Xiangyu Yang†, Xuankai Wang†, Yawen Zou, Shilong Zhang, Manying Xia, Lianting Fu, Mitchell R. Vollger, Nae-Chyun Chen, Dylan J. Taylor, William T. Harvey, Glennis A. Logsdon, Dan Meng, Junfeng Shi, Rajiv C. McCoy, Michael C. Schatz, Weidong Li, Evan E. Eichler, Qing Lu, Yafei Mao*

*Corresponding author: yafmao@sjtu.edu.cn

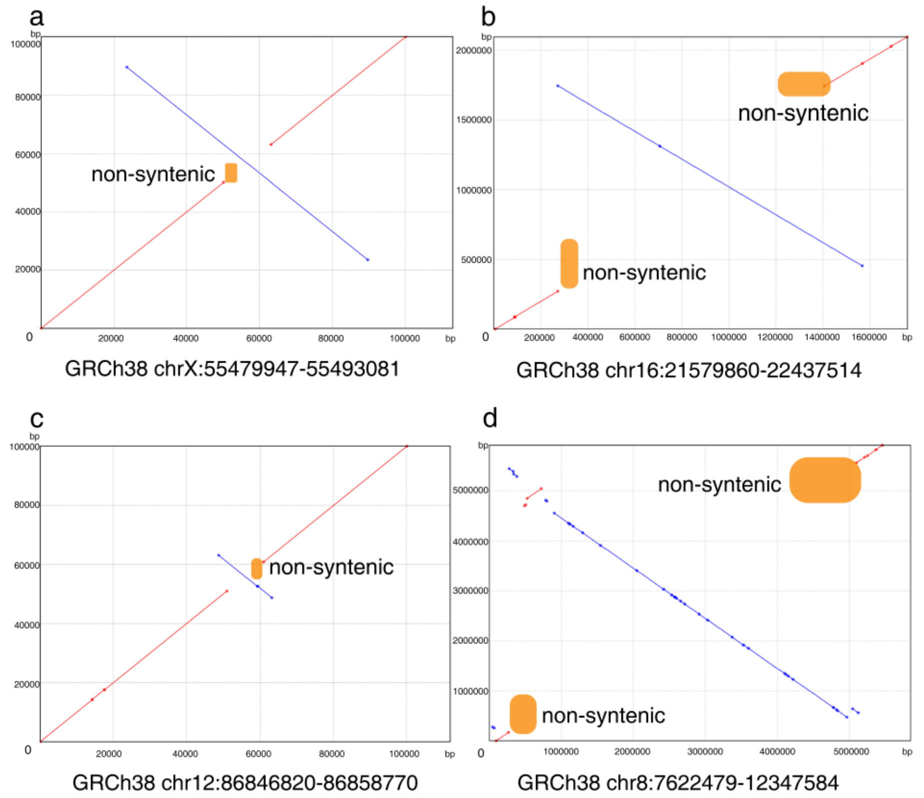

Fig. S1. The visualization of four discrepant regions by dotplot. The dotplots of the four different large-scale discrepant regions containing six ‘non-syntenic’ regions. The previous studies found the breakpoint of those inversions (orange area) rather than the whole inversion coordinate. The x-axis represents the GRCh38 coordinate and the y-axis represents the T2T-CHM13 coordinate. GRCh38 inversions shown for (a) chrX:55479947-55493081, (b) chr16:21579860-224437514, (c) chr12:86846820-86858770, and (d) chr8:7622479-12347584.

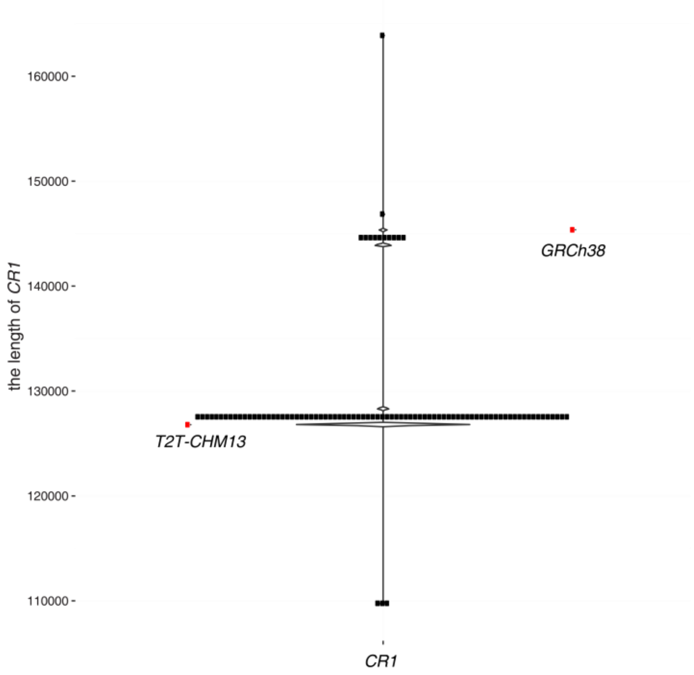

Fig. S2. Comparison of the gene length of *CR1* in long-read human genome assemblies. The violin plot shows the distribution of *CR1* length in the 94 long-read human genome assemblies. Red dots indicate *CR1*_gene length in T2T-CHM13 and GRCh38. Black dots indicate the length of *CR1* in the 94 long-read human genome assemblies.

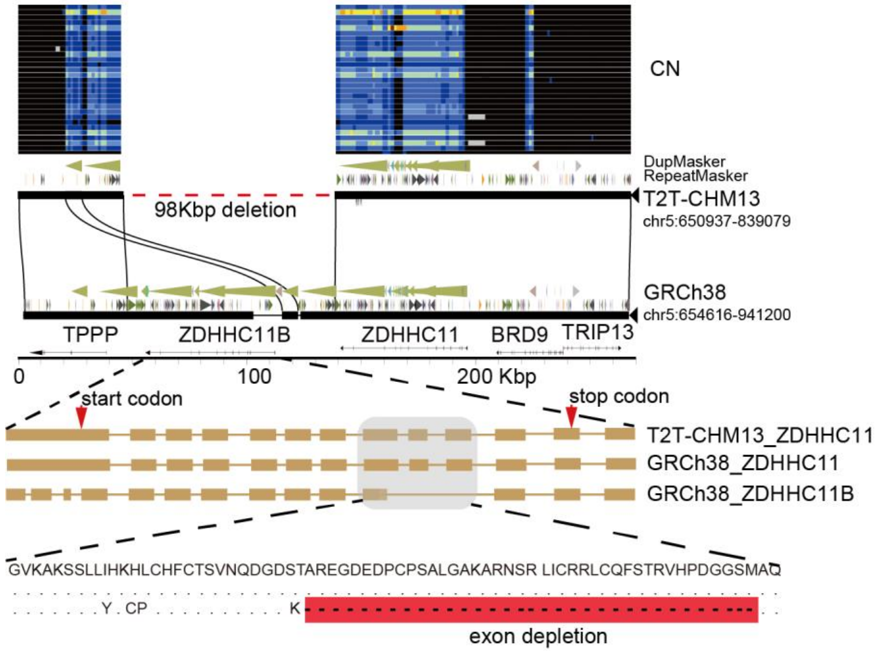

Fig. S3. Gene structure differences in the discrepant regions. The depletion of ZDHHC11B in the T2T-CHM13 genome assembly by a ~98 kbp deletion. The CN heatmap inferred from SGPD is shown in the top panel. The miropeat synteny relationship shows structural variation with repeat, duplication, and gene annotation. The exon schematic with amino acid alignment shows the gene model difference in the two assemblies.

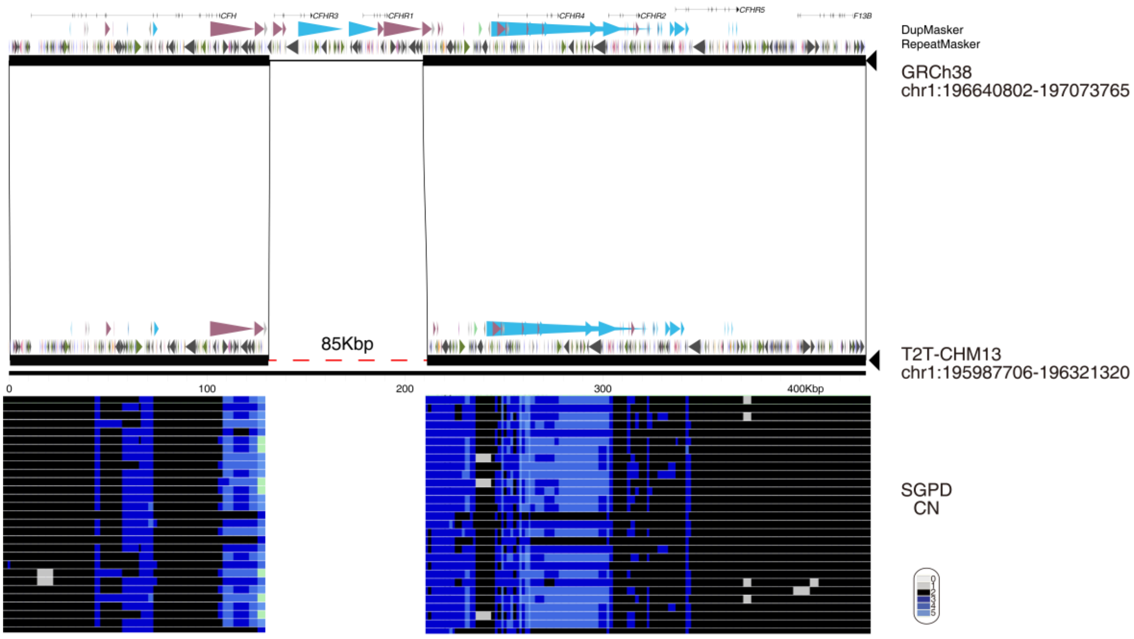

Fig. S4. The discrepant region contains *CFHR1* and *CFHR3*. The depletion of *CFHR1* and *CFHR3* by an 85 kbp deletion variant. The CN heatmap shows the CN of the discrepant region.

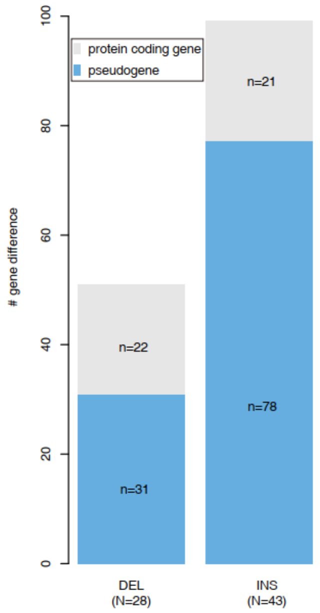

Fig. S5. The number of gene difference in deletions (total *N* = 68) and insertions (total *N* = 87) between GRCh38 and T2T-CHM13. Barplot shows the number of genes different (Y axis) in discrepant genomic regions between GRCh38 and T2T-CHM13. 28 deletion regions (*N* = 28, 28/68) and 43 insertion regions (*N* = 43, 43/87) include 53 genes (22 protein coding genes and 31 pseudogenes) and 99 genes (21 protein coding genes and 78 pseudogenes), respectively.

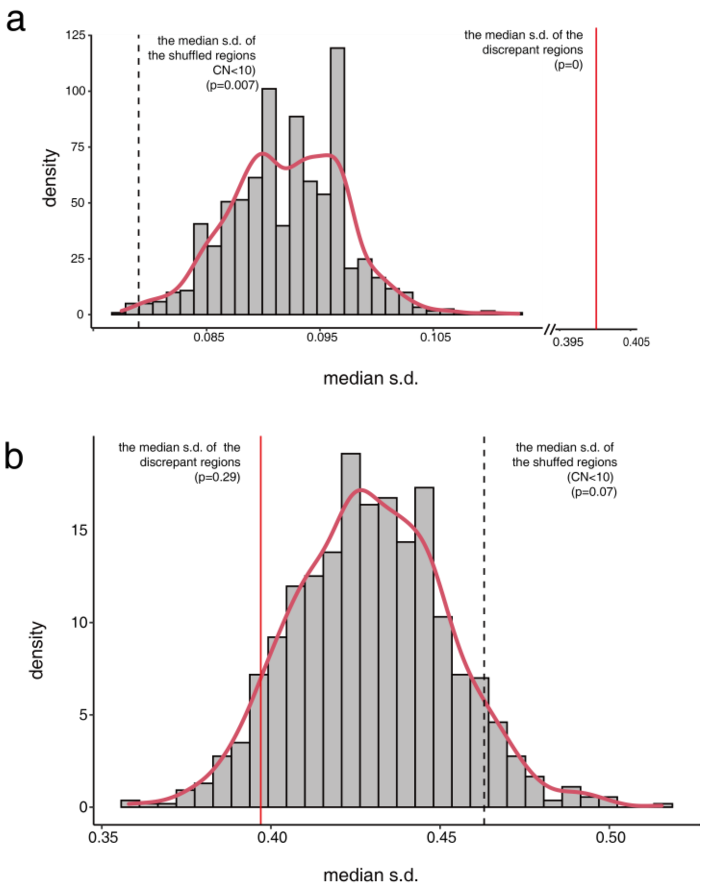

Fig. S6. The distribution of the median CN s.d. (a) Median s.d. of the 131 discrepant regions is significantly higher than the whole genome-wide simulation. (b) No significant difference between the median CN s.d. of the 131 discrepant regions (median=0.46) and that of the CN variable genomic regions (median=0.4, empirical p=0.07).

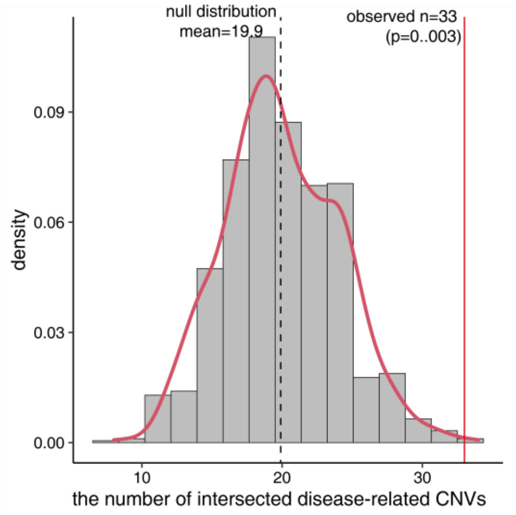

Fig. S7. The distribution of intersected disease-related CNVs. With genome-wide permutation analysis, we found some discrepant regions are more likely associated with the reported disease-related CNVs.

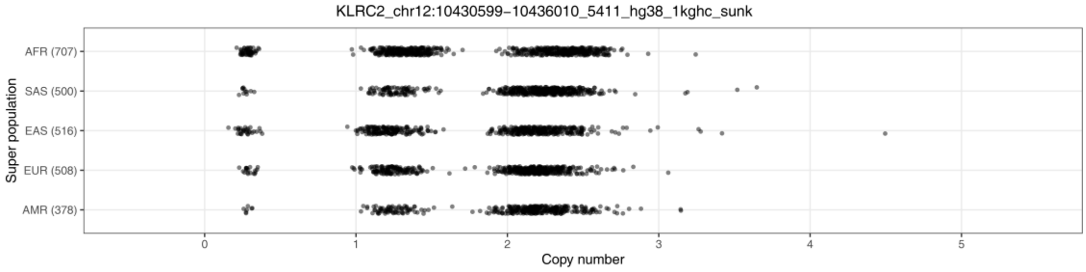

Fig. S8. The SGPD read-depth genotyping of *KLRC2* in different human populations. The CN of *KLRC2* in different populations present the CN polymorphism.

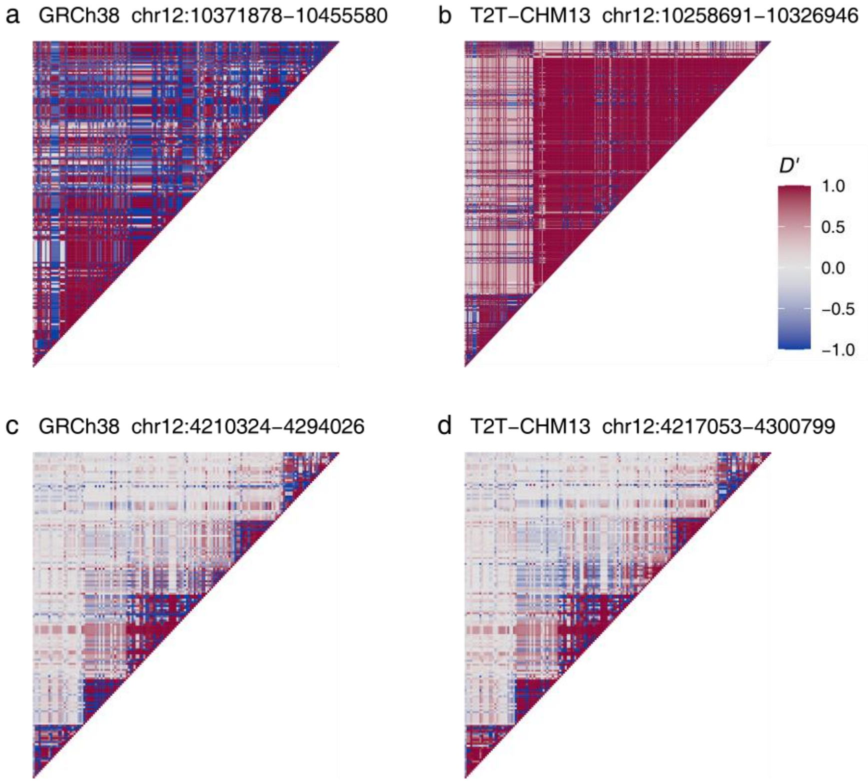

Fig. S9. The haplotype structure of living human populations in T2T-CHM13. LD at the *KLRC* locus extends much farther than the randomly selected control locus, which exhibits multiple, shorter haplotype blocks, potentially reflecting differences in the history of recombination within the regions.

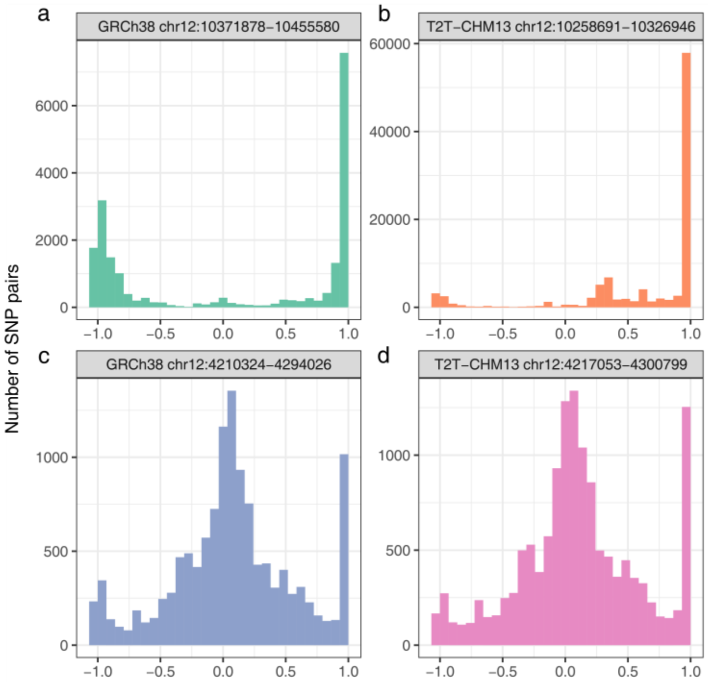

Fig. S10. SNV distribution in T2T-CHM13 and GRCh38 of two chromosome regions. Regions shown are (a) GRCh38 chr12:10371878-10455580, (b) T2T-CHM13 chr12:10258691-10326946, (c) GRCh38 chr12:4210324-4194026, and (d) T2T-CHM13 chr12:4217053-4300

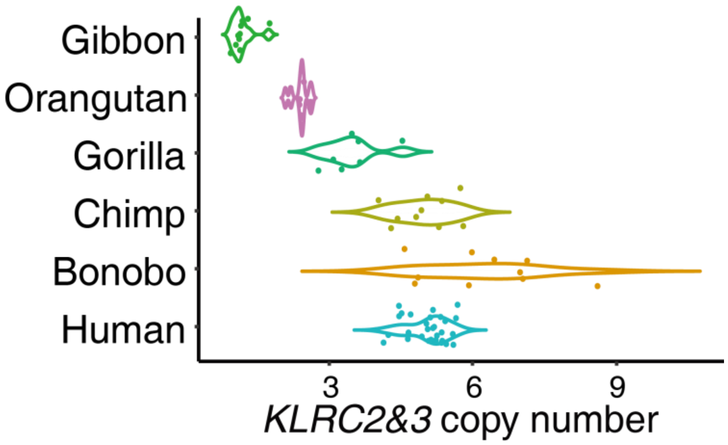

Fig. S11. CN of *KLRC2* and *KLRC3* for NHP population level. African great apes show the highest CN of *KLRC2* and *KLRC3* versus other primates.

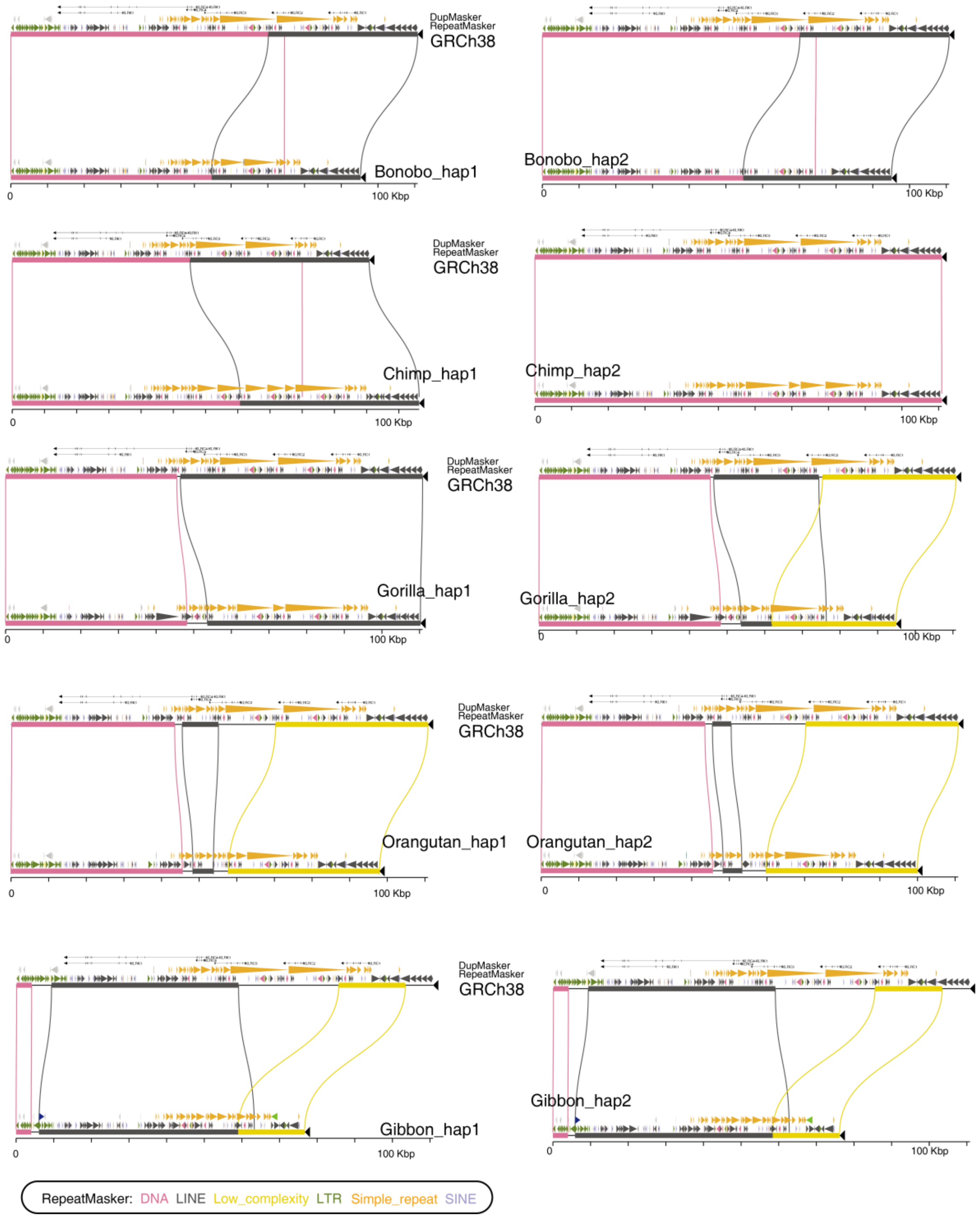

Fig. S12. The syntenic relationship of *KLRC* gene cluster region between human and different apes. *KLRC2* and *KLRC3* are deleted in two gibbon genome assemblies.

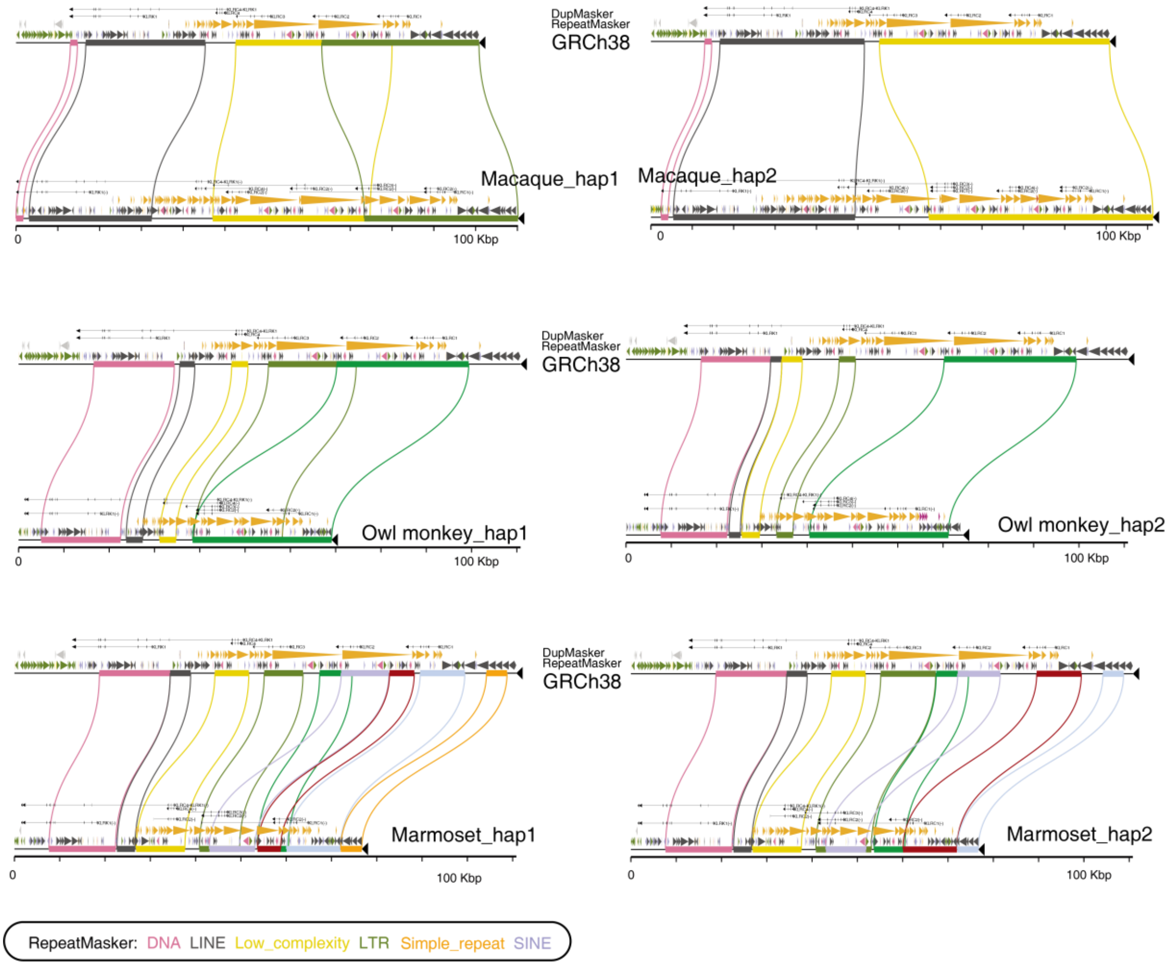

Fig. S13. The syntenic relationship of *KLRC* gene cluster region between human and monkey genomes. The duplication of *KLRC2* is found in macaques.

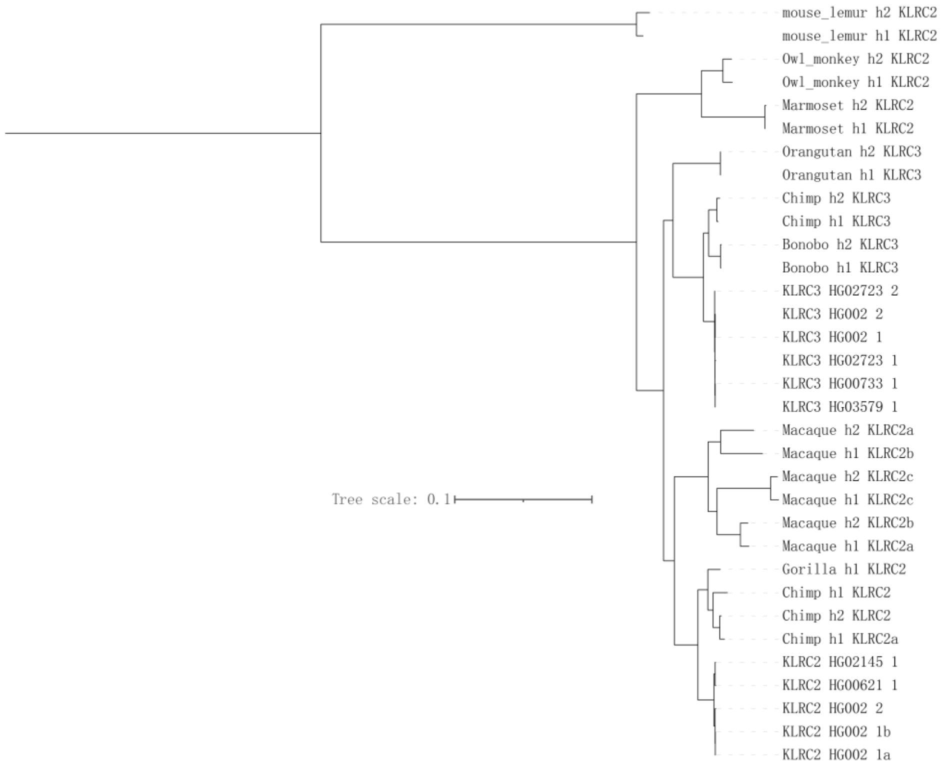

Fig. S14. The phylogenetic tree of *KLRC2* and *KLRC3* with mouse lemur as outgroup. The phylogenic tree of *KLRC2* and *KLRC3* with ~5.5 kbp genomic region suggests *KLRC2* and *KLRC3* are duplicated at the common ancestor of apes and Old-World monkey.

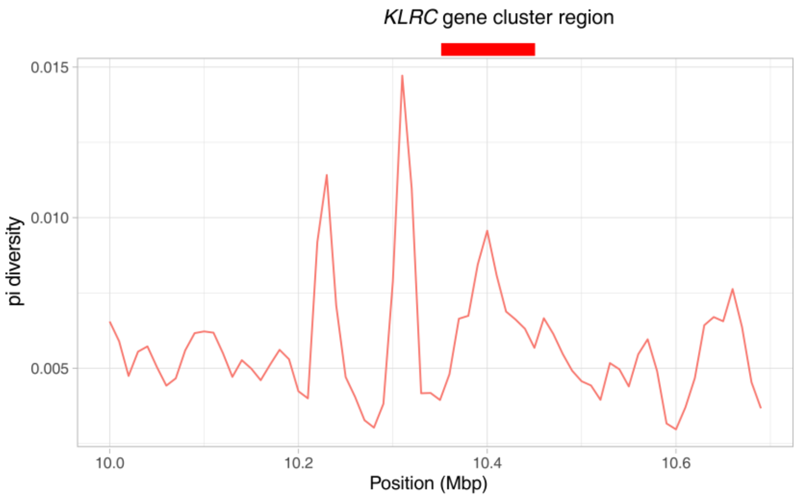

Fig. S15. The pi diversity of the *KLRC* gene cluster based on the 94 long-read genome assemblies. We did not obverse any significant pi diversity changes in the region. The red box represents the *KLRC* gene cluster region.

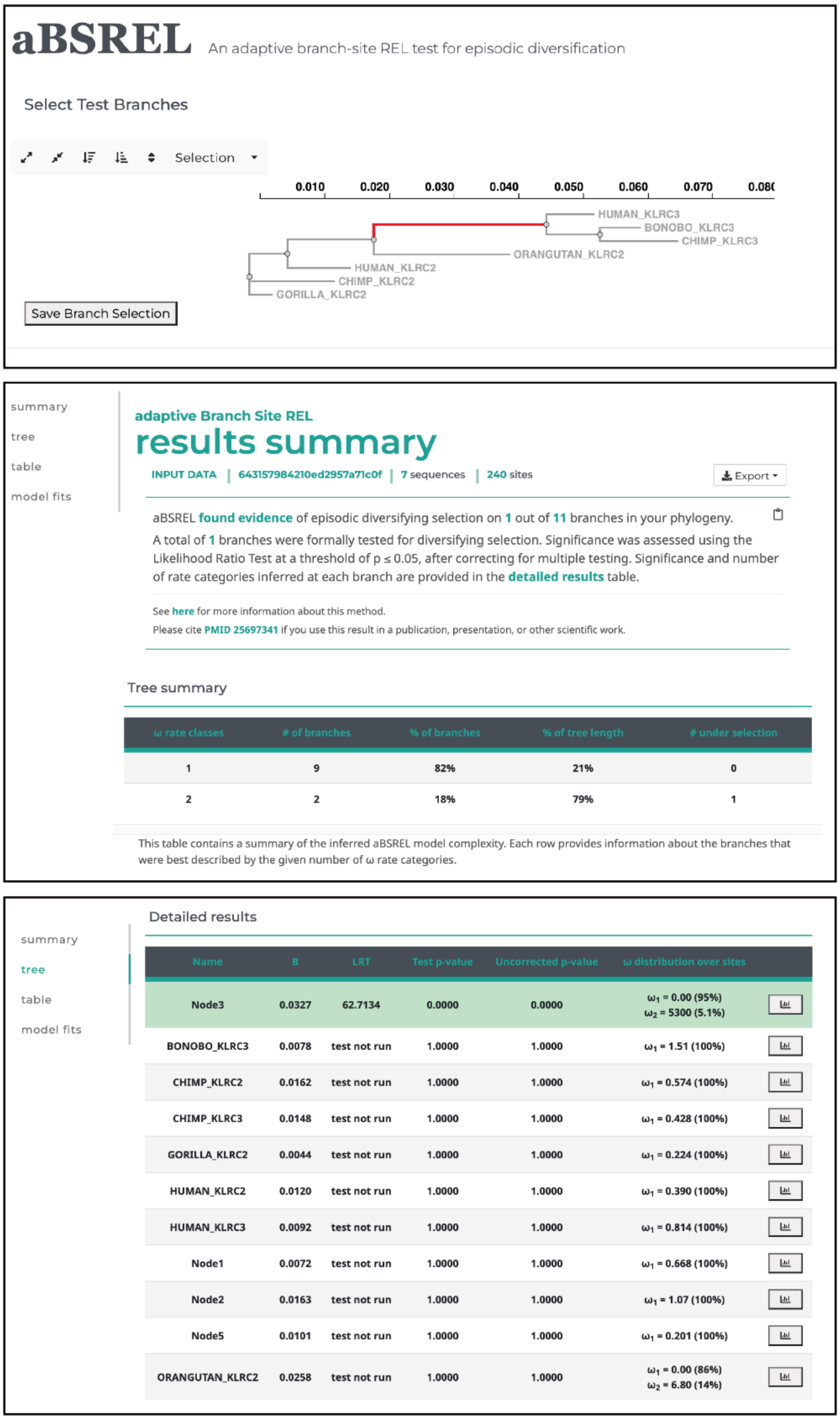

adaptive Branch Site REL

results summary

INPUT DATA | 643157984210ed2957a71c0f | 7 sequences | 240 sites

aBSREL **found evidence** of episodic diversifying selection on **1** out of **11** branches in your phylogeny.

A total of **1** branches were formally tested for diversifying selection. Significance was assessed using the Likelihood Ratio Test at a threshold of p ≤ 0.05, after correcting for multiple testing. Significance and number of rate categories inferred at each branch are provided in the **detailed results** table.

See **here** for more information about this method.

Please cite **PMID 25697341** if you use this result in a publication, presentation, or other scientific work.

Tree summary

ω rate classes	# of branches	% of branches	% of tree length	# under selection
1	9	82%	21%	0
2	2	18%	79%	1

This table contains a summary of the inferred aBSREL model complexity. Each row provides information about the branches that were best described by the given number of ω rate categories.

Detailed results

Name	B	LRT	Test p-value	Uncorrected p-value	ω distribution over sites	
Node3	0.0327	62.7134	0.0000	0.0000	ω_1 = 0.00 (95%) ω_2 = 5300 (5.1%)	
BONOBO_KLRC3	0.0078	test not run	1.0000	1.0000	ω_1 = 1.51 (100%)	
CHIMP_KLRC2	0.0162	test not run	1.0000	1.0000	ω_1 = 0.574 (100%)	
CHIMP_KLRC3	0.0148	test not run	1.0000	1.0000	ω_1 = 0.428 (100%)	
GORILLA_KLRC2	0.0044	test not run	1.0000	1.0000	ω_1 = 0.224 (100%)	
HUMAN_KLRC2	0.0120	test not run	1.0000	1.0000	ω_1 = 0.390 (100%)	
HUMAN_KLRC3	0.0092	test not run	1.0000	1.0000	ω_1 = 0.814 (100%)	
Node1	0.0072	test not run	1.0000	1.0000	ω_1 = 0.668 (100%)	
Node2	0.0163	test not run	1.0000	1.0000	ω_1 = 1.07 (100%)	
Node5	0.0101	test not run	1.0000	1.0000	ω_1 = 0.201 (100%)	
ORANGUTAN_KLRC2	0.0258	test not run	1.0000	1.0000	ω_1 = 0.00 (86%) ω_2 = 6.80 (14%)	

Fig. S16. Selection pressure testing using aBSREL on *KLRC3* clade. The aBSREL model suggested that node 2 is under selection with a *p*-value of $\leqslant$ 0.05.

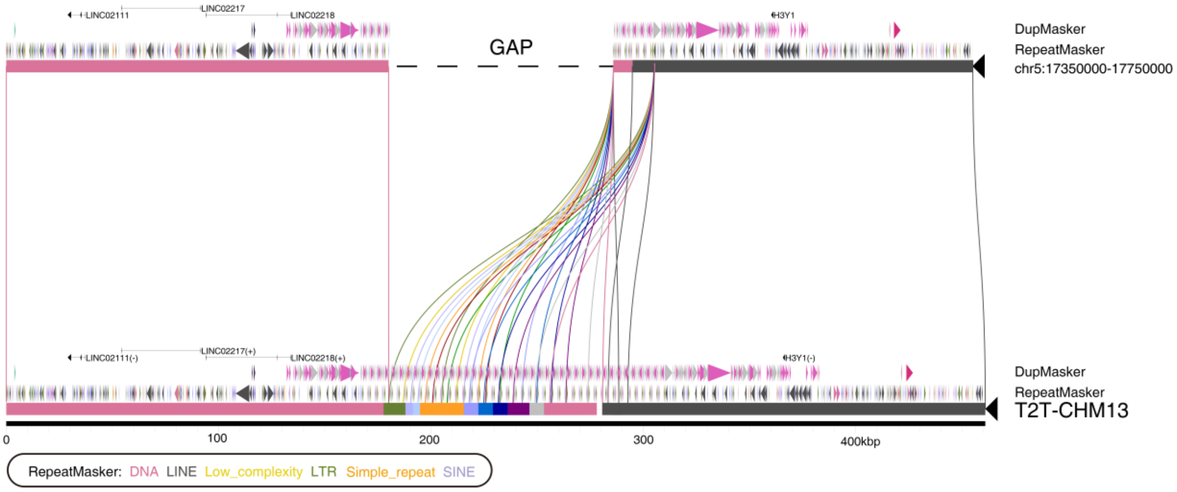

Fig. S17. Comparison of the genomic region of the inversion containing a gap in GRCh38. The miropeat synteny relationship of the region shows an inversion between GRCh38 and T2T-CHM13. There is a gap in GRCh38 resulting in a false negative call in the previous study.

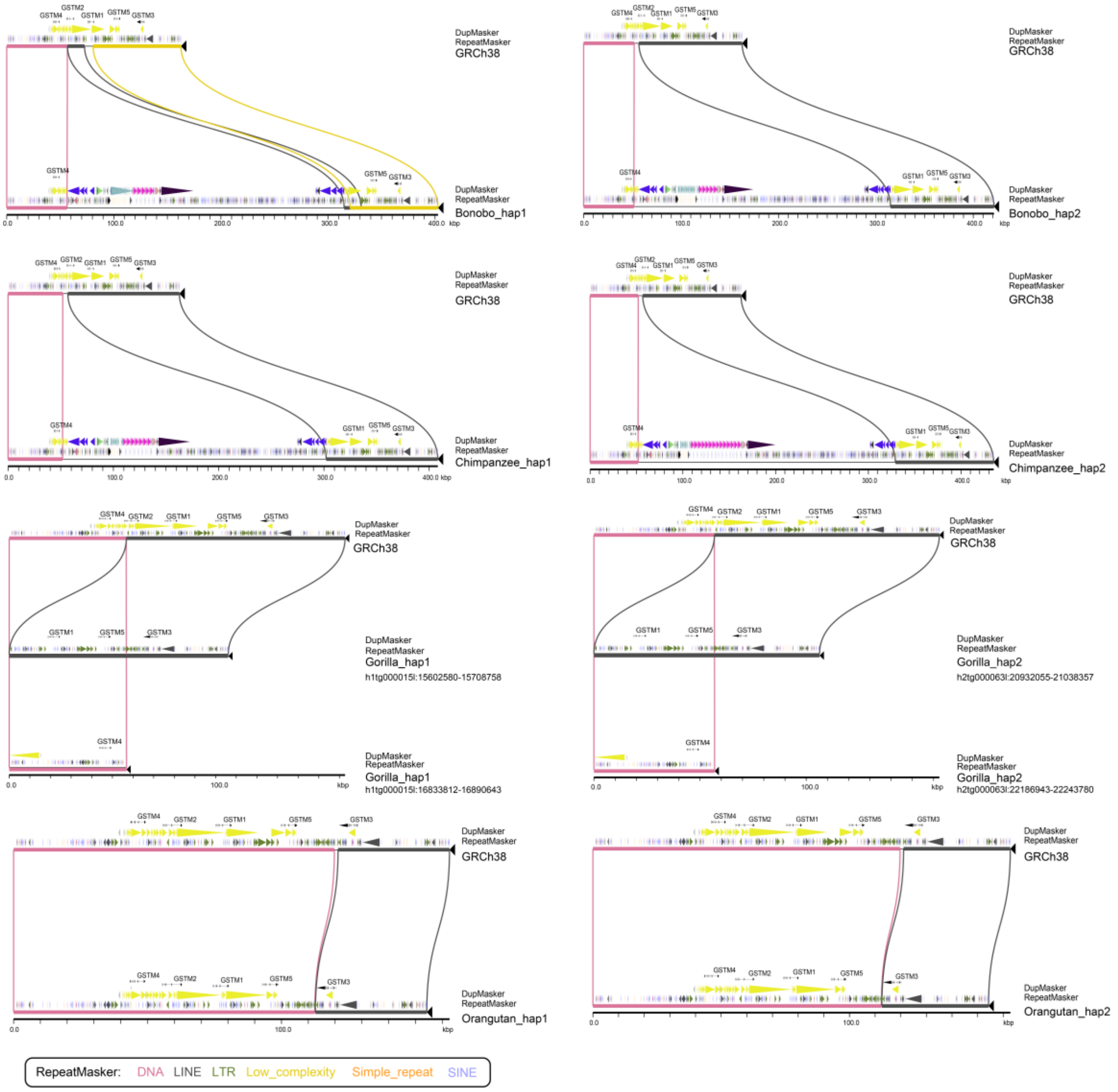

Fig. S18. The syntenic relationship of *GSTM* gene cluster region between human and NHPs. The copy number *GSTM* is variable in primates and *GSTM2* is deleted in chimpanzee, bonobo, and gorilla genome assemblies.

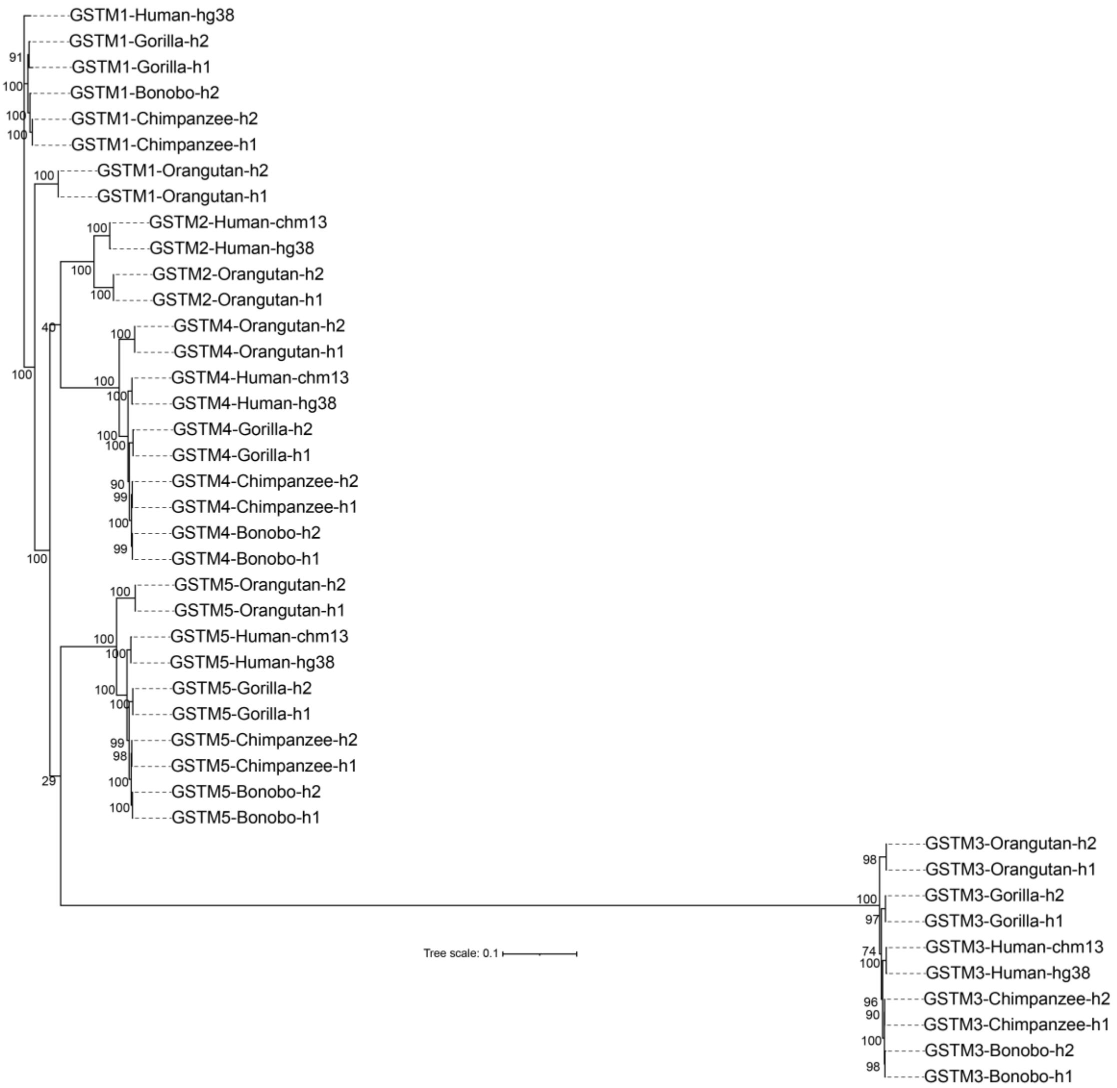

Fig. S19. The phylogenetic tree of *GSTM* in primates. The phylogenetic tree of *GSTM* reconstructed with 4.1 kbp genomic regions suggests that *GSTM1* and *GSTM2* gene recurrently mutated during primate evolution.

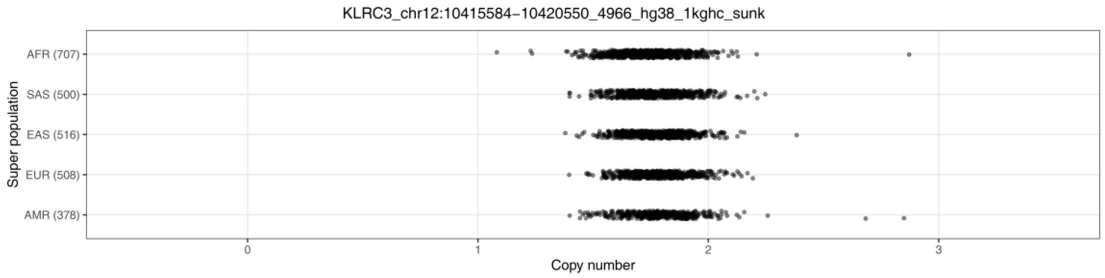

Fig. S20. The CN of *KLRC3* in different human populations. The result of the SGPD read depth genotyping suggests there is no CN variation of *KLRC3* in humans.